Value Adding Products derived from the ATCOR Models

(Version 5.5, January 2003)

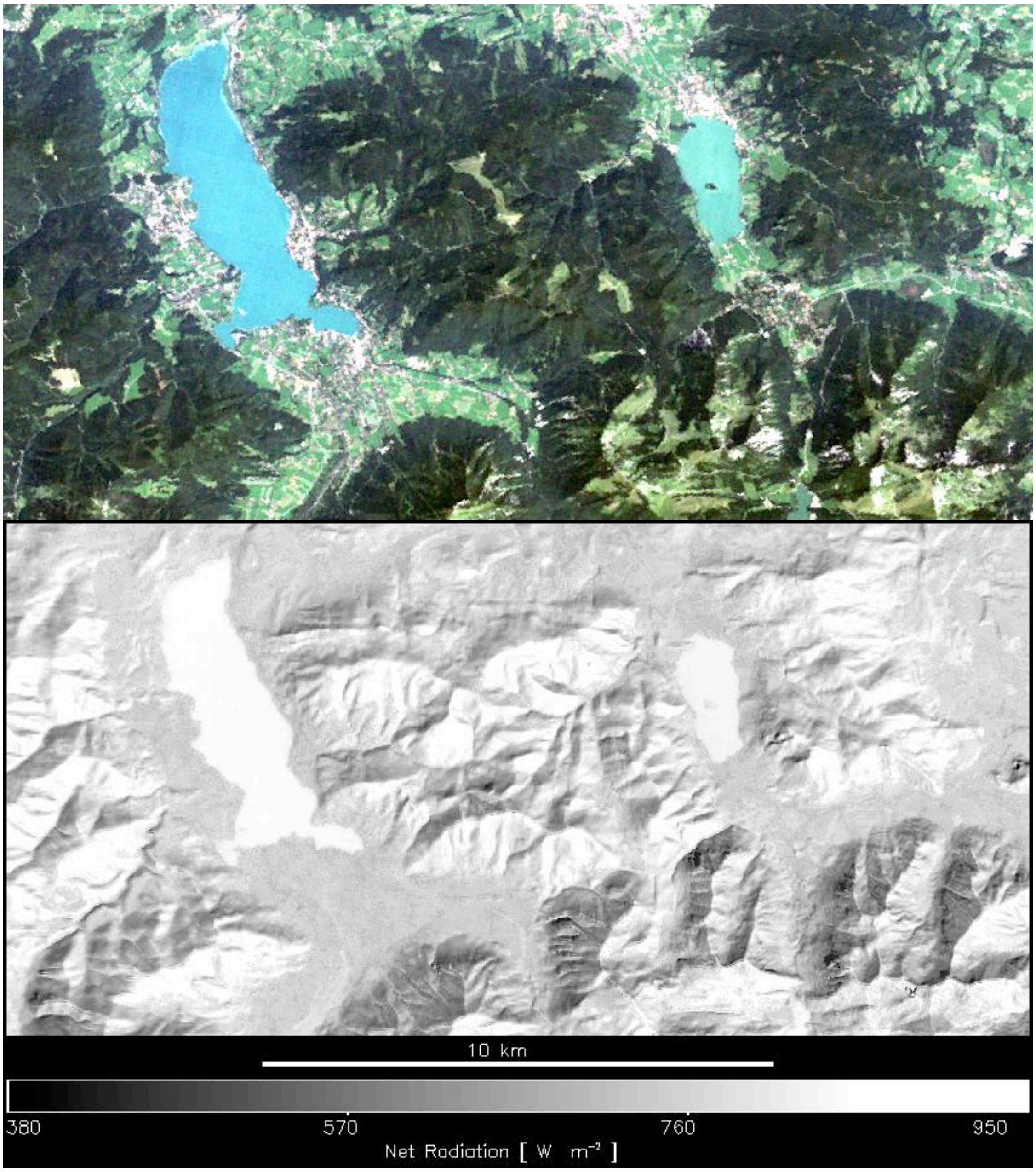

R. Richter
DLR – German Aerospace Center
Remote Sensing Data Center
D - 82234 Wessling / Germany

DLR-IB 564-03/03
(Report of Institute IMF)

The cover image shows the net radiation calculated for a Landsat-5 TM sub-scene near Munich covering some lakes and part of the Alps. A digital elevation model is employed in the derivation of surface reflectance to correct for atmospheric and topographic effects.

Net radiation is high for water bodies and for surfaces oriented toward the sun. Lower values of net radiation occur for high-reflectance and high-temperature surfaces as well as for surfaces oriented away from the sun.

The imagery of net radiation is one channel of several value adding channels that can be calculated as an option in the ATCOR models.

The cover image is based on a selected Thematic Mapper (TM) scene taken from a set of multitemporal Landsat TM scenes (1985 – 1997) of alpine areas that were processed in the framework of ALPMON, an alpine monitoring project sponsored by the European Community.

Contents

Figures

Tables

1. Introduction

Remotely sensed imagery of spaceborne sensors covers large areas of the earth's surface nearly at the same time. The combination of this information with point-like local measurements of meteorological data is indispensible for applications in climatology, monitoring of change detection, agriculture, and forestry. This report describes some products that can be derived from atmospherically corrected imagery of optical sensors, i.e., based on surface reflectance and temperature data. The derivation of these value adding products is an option for the airborne and satellite versions of the ATCOR model (Richter 1996, 1997, 1998, 2003a, 2003b).

The first group of products include a vegetation index (SAVI), the leaf area index (LAI), the fraction of absorbed photosynthetically active radiaton (FPAR), and ground albedo, i.e. the ground reflectance integrated over the wavelength region 0.3 – 2.5 μm. The second group comprises quantities relevant for surface energy balance such as absorbed solar radiation flux, surface emitted thermal flux and thermal air-to-surface flux, and net radiation. It requires sensors with at least one thermal band.

A simple model based on the SAVI vegetation index is employed to calculate the leaf area index and the heat flux into the ground. The sensible and latent heat flux are calculated with an approach proposed by Carlson et al. (1995). The sensible heat flux is computed with the scaled normalized difference vegetation index (scaled NDVI). The justification for the simple approach is that these heat fluxes depend on a number of micrometeorological parameters (thermal properties of soil, surface roughness, wind velocity, etc.) that are usually not known. Nevertheless, the simple model is able to provide reasonable flux values over large vegetated areas covered by a satellite sensor. It can be a useful complement to local detailed field campaign measurements.

Several multitemporal Landsat TM scenes (1985 – 1997) of alpine areas were processed in the framework of ALPMON, an alpine monitoring project sponsored by the European Community. The ALPMON sample imagery and digital elevation data presented here was kindly provided by Dr. Schneider, University of Munich, Institute for Land Use Planning and Nature Conservation (ALPMON project 1996). The second scene is selected from a flat region. It contains the city of Munich. Although these examples present satellite imagery the same type of processing is also available for airborne imagery.

The following two panels show ATCOR's graphical user interface for the value adding channels if the sensor has at least one thermal band.

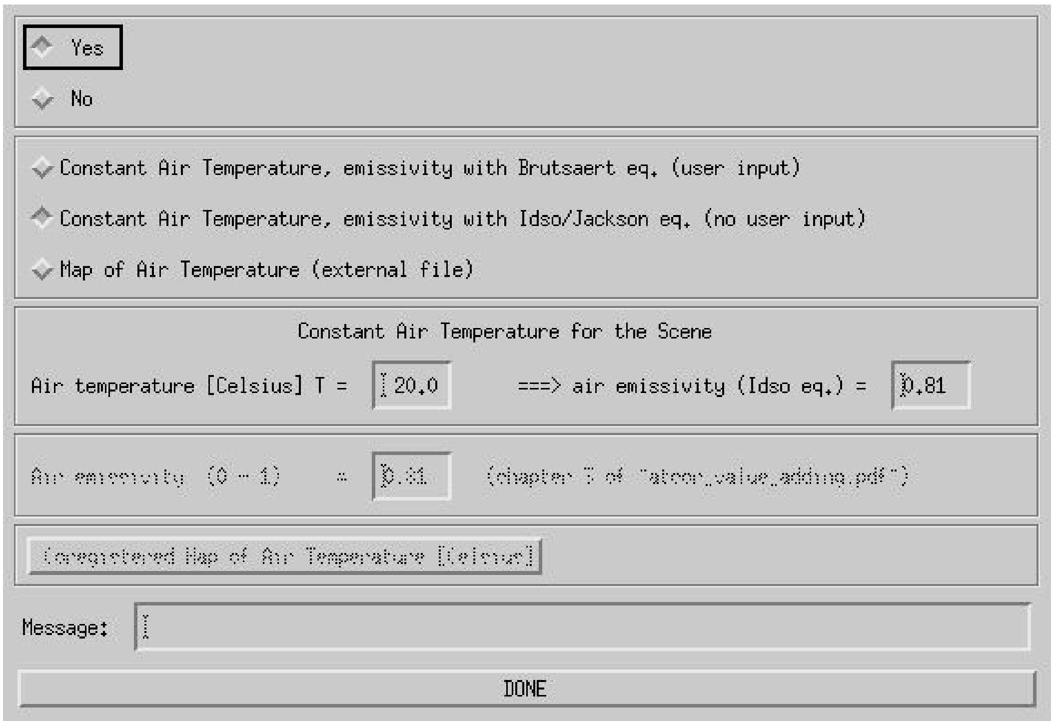

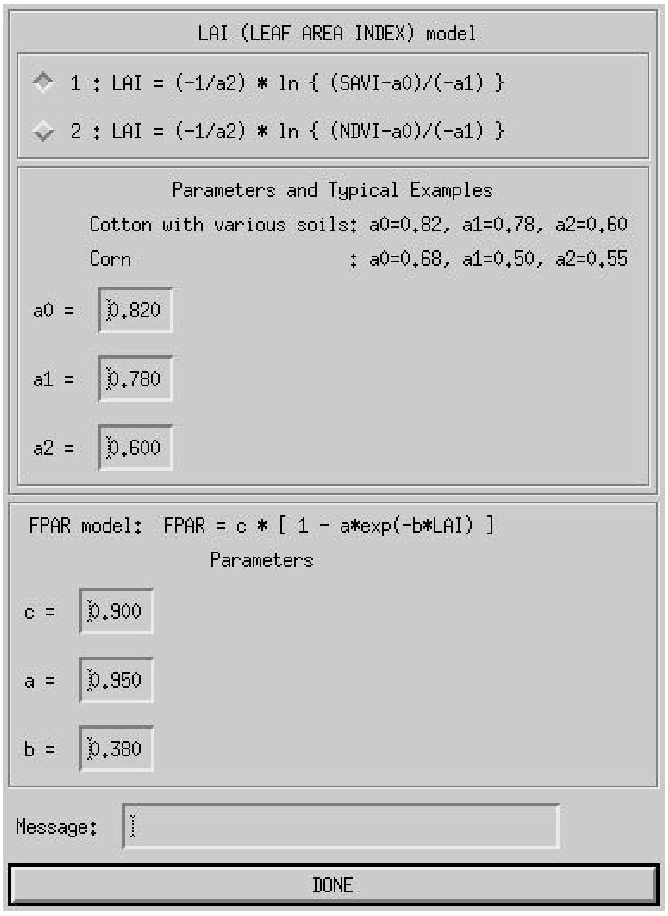

2. Vegetation Index, Leaf Area Index, FPAR, Ground Albedo

The first group of value adding products consists of the following channels:

- The soil adjusted vegetation index (SAVI) defined as (Huete 1988, Baret and Guyot 1991)

$$SAVI = \frac{(\rho_{NIR} - \rho_{RED}) \cdot 1.5}{\rho_{NIR} + \rho_{RED} + 0.5} \tag{2.1}$$

where ρ_{RED} and ρ_{NIR} are ground reflectance values for a red (650 nm) and near-infrared (850 nm) band, respectively.
The SAVI index was selected from a variety of vegetation indices because it is suitable to parametrize the leaf area index (LAI), the fraction of absorbed photosynthetically active radiation (FPAR) and surface energy fluxes (Baret and Guyot 1991, Choudhury 1994). The range of SAVI is 0 – 1.

- The leaf area index (LAI): an empirical relation between LAI and a vegetation index VI (VI=SAVI or VI=NDVI) with three parameters is used (Asrar et al. 1984, Baret and Guyot 1991) :

$$VI = a_0 - a_1 \ exp\,(-a_2 \cdot LAI\,)$$

Solving for LAI one obtains

$$LAI = -(1/\,a_2\,)\ ln \left(\frac{a_0 - VI}{a_1} \right) \tag{2.2}$$

Sample sets of parameters are $a_0 = 0.82, a_1 = 0.78, a_2 = 0.6$ (cotton with varied soil types), $a_0 = 0.68, a_1 = 0.50, a_2 = 0.55$ (corn), and $a_0 = 0.72, a_1 = 0.61, a_2 = 0.65$ (soybean) with VI=SAVI (Choudury et al. 1994).

- The FPAR channel: Plants absorb solar radiation mainly in the 0.4-0.7 μm region (PAR region, photosynthetically active radiation, Asrar 1989). The absorbed photosynthetically active radiation is called APAR, and the fraction of absorbed photosynthetically active radiation is abbreviated as FPAR. These terms are associated with the green phytomass and crop productivity. A three-parameter model can be employed to approximate APAR and FPAR (Asrar et al. 1984, Asrar 1989, Wiegand et al. 1990, 1991).

$$FPAR = C \left[1 - A\ exp\,(-B \cdot LAI\,) \right] \tag{2.3}$$

Typical values are C=1, A=1, B=0.4.

Equations (2.1) to (2.3) can be the basis for user-customized additional evaluations, e.g., crop yield estimation (Wiegand et al. 1991).

- The ground albedo: the wavelength-integrated ground reflectance (a directional-hemispherical reflectance) is used as a substitute for surface albedo (bi-hemispherical reflectance). It is calculated as

$$a = \frac{\int_{0.3\mu m}^{2.5\mu m} \rho(\lambda)\, d\lambda}{\int_{0.3\mu m}^{2.5\mu m} d\lambda} \tag{2.4}$$

Since most satellite sensors cover only part of the 0.3 – 2.5 μm region the following assumptions are being made to extrapolate the available region :

- $\rho_{0.3-0.4\mu m} = 0.8 \cdot \rho_{blue}$, and $\rho_{0.3-0.4\mu m} = 0.8 \cdot \rho_{green}$, if a blue band does not exist.
- $\rho_{0.4-0.45\mu m} = 0.9 \cdot \rho_{blue}$, and $\rho_{0.4-0.52\mu m} = 0.9 \cdot \rho_{green}$ (no blue band available).

The extrapolation to longer wavelength bands is computed as:
A) If a 1.6 μm band is available :

- $\rho_{2.0-2.5\mu m} = 0.5 \cdot \rho_{1.6\mu m}$ (vegetation with $\rho_{NIR} / \rho_{Red} > 3$)
- $\rho_{2.0-2.5\mu m} = \rho_{1.6\mu m}$ (else)

B) If no bands at 1.6 and 2.2 μm are available the contribution for these regions is estimated as:

- $\rho_{1.5-1.8\mu m} = 0.50 \cdot \rho_{0.85\mu m}$ (vegetation with $\rho_{NIR} / \rho_{Red} > 3$)
- $\rho_{2.0-2.5\mu m} = 0.25 \cdot \rho_{0.85\mu m}$ (vegetation with $\rho_{NIR} / \rho_{Red} > 3$)
- $\rho_{1.5-1.8\mu m} = \rho_{0.85\mu m}$ (else)
- $\rho_{2.0-2.5\mu m} = \rho_{0.85\mu m}$ (else)

At least three bands in the green, red, and near-infrared are required to derive the albedo product. Wavelength gap regions are supplemented with interpolation.
The contribution of the 2.5-3.0 μm region is neglected here.

The file containing the channels of SAVI, LAI, FPAR, and surface albedo is coded with 2 bytes per pixel, and employs the following scale factors:

- SAVI: range 0 – 1000, scale factor 1000, so scaled SAVI=500 corresponds to SAVI=0.5 .
- LAI : range 0 – 10000, scale factor 1000, so scaled LAI=5000 corresponds to LAI=5 .
- FPAR: range 0-1000, scale factor 1000, so scaled FPAR=500 corresponds to FPAR=0.5 .
- Albedo: range 0-1000, scale factor 10, so scaled albedo=500 corresponds to albedo=50% .

2.1 Landsat-5 TM scene (ALPMON 1985)

Figures 2.1 to 2.4 show the image products of SAVI, LAI, ground (brightness) temperature (for emissivity 0.98) and surface albedo for the ALPMON 1985 scene. The scene was acquired on 13 August 1985, the solar zenith angle is 40°, the solar azimuth angle is 136.8°. The FPAR channel is strongly correlated to SAVI and not shown.

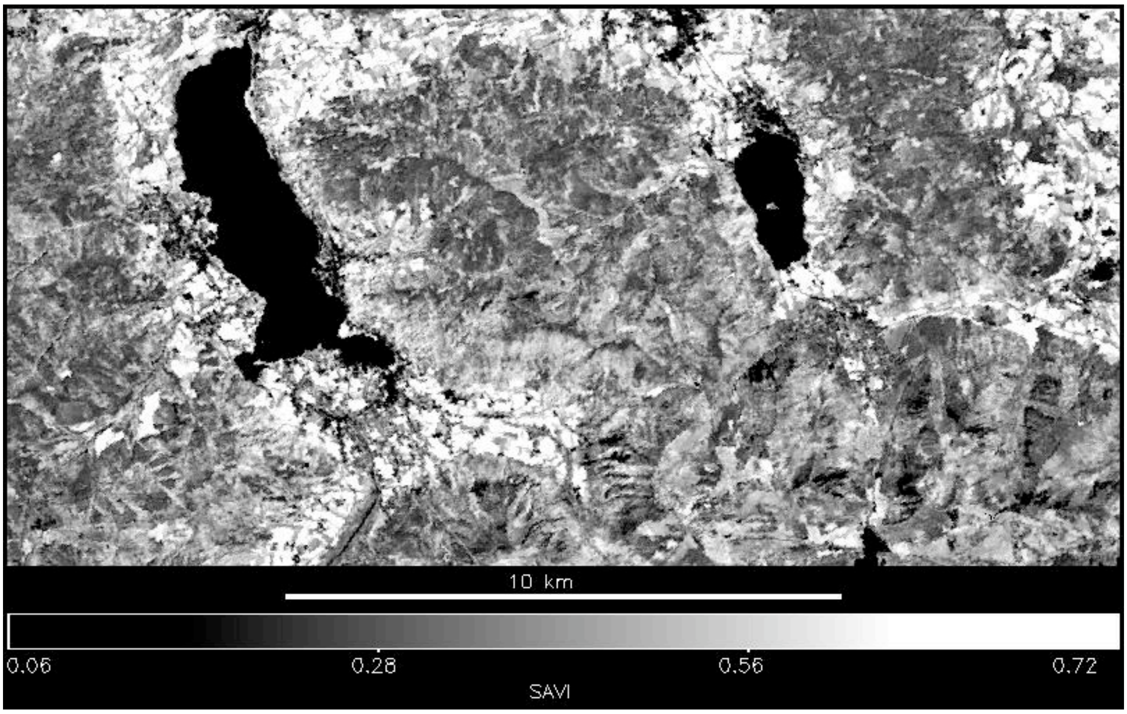

Figure 2.1 SAVI channel of the TM scene corresponding to the title imagery.

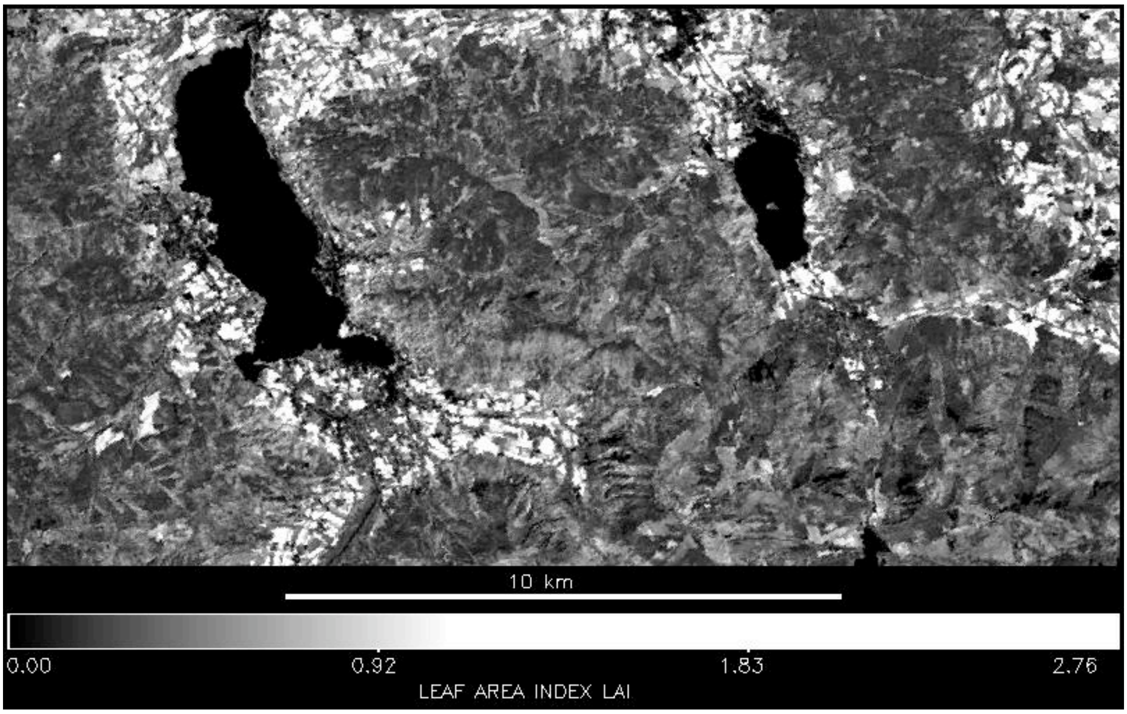

Figure 2.2 Leaf area index channel.

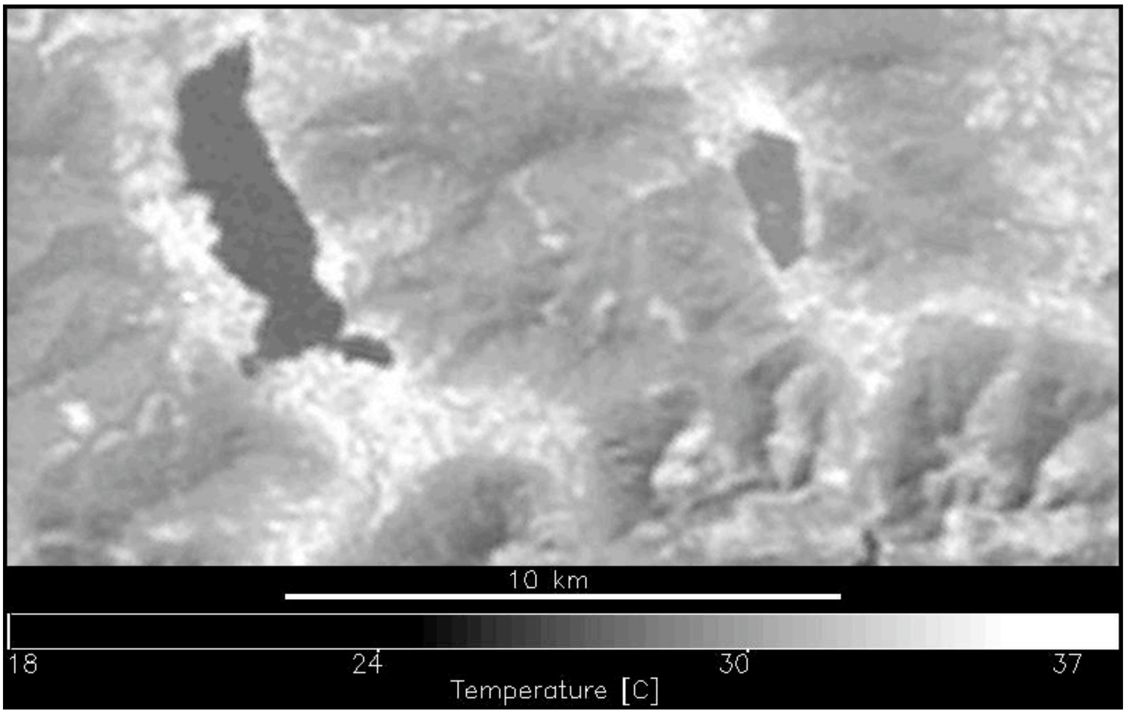

Figure 2.3 Ground brightness temperature channel (120 m resolution of thermal band).

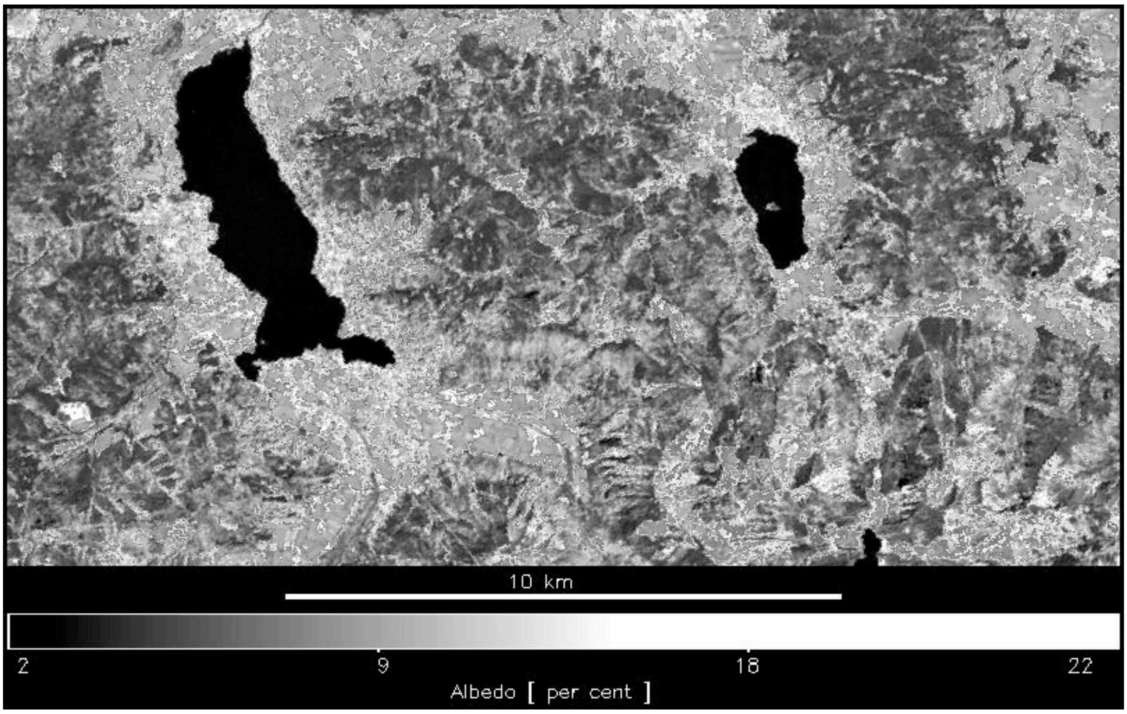

Figure 2.4 Surface albedo channel (30 m resolution of bands in the solar region).

2.2 Landsat-5 TM scene (Munich 1991)

Figure 2.5 shows part of a Landsat-5 TM scene of Munich acquired on 29 September 1991. The solar zenith angle for this scene is 46°. The area is flat, so no digital elevation model was used here. Figures 2.6 to 2.9 show the computed image products of SAVI, LAI, ground (brightness) temperature (for emissivity 0.98) and albedo.

Figure 2.5 TM scene of Munich (bands 3,2,1 coded red, green, blue).

Figure 2.6 SAVI channel of the TM scene.

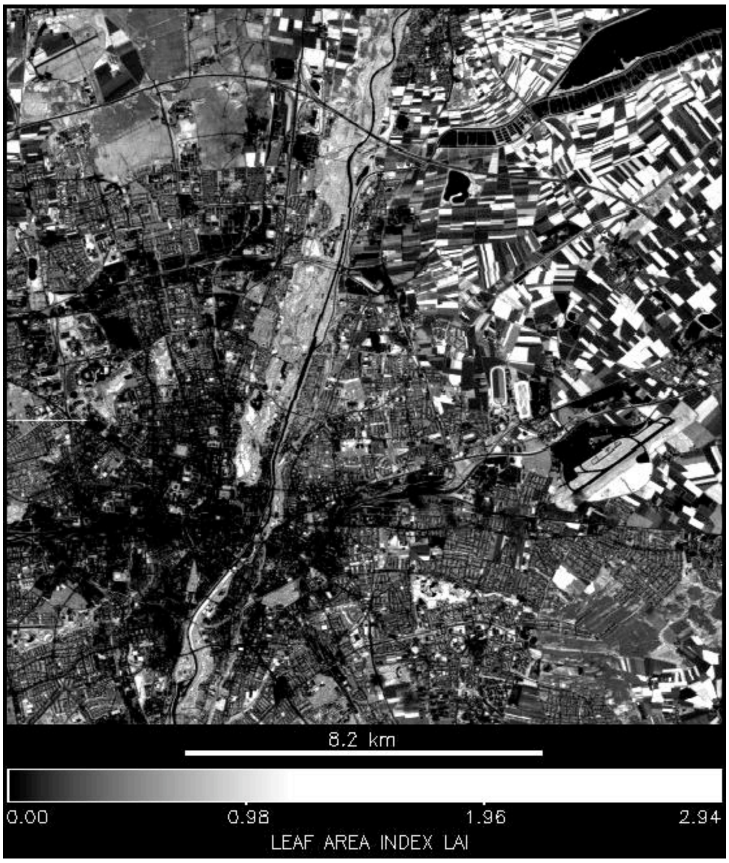

Figure 2.7 Leaf area index channel.

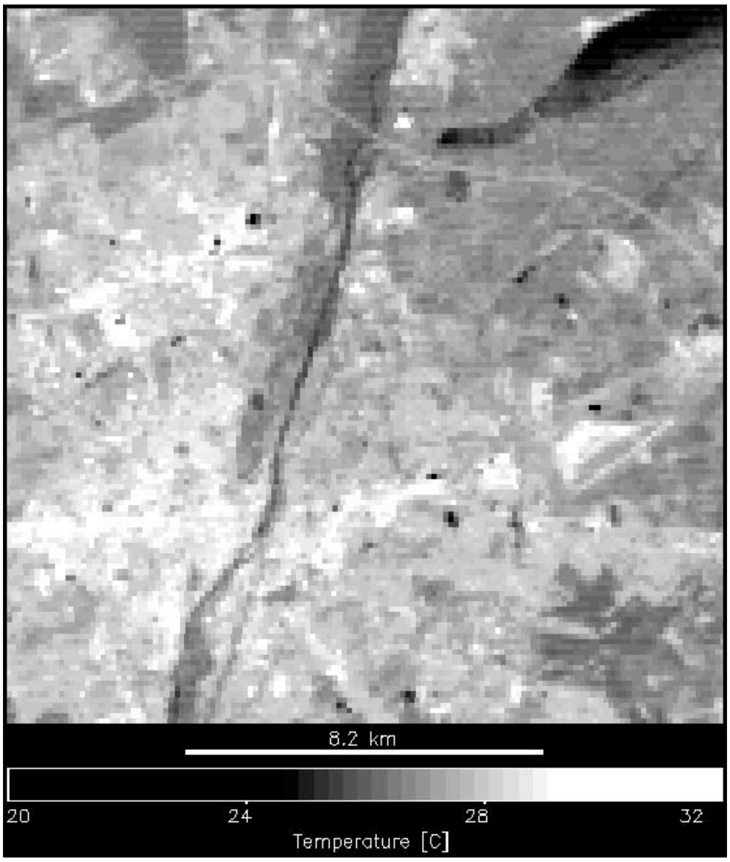

Figure 2.8 Ground brightness temperature channel (120 m resolution of thermal band).

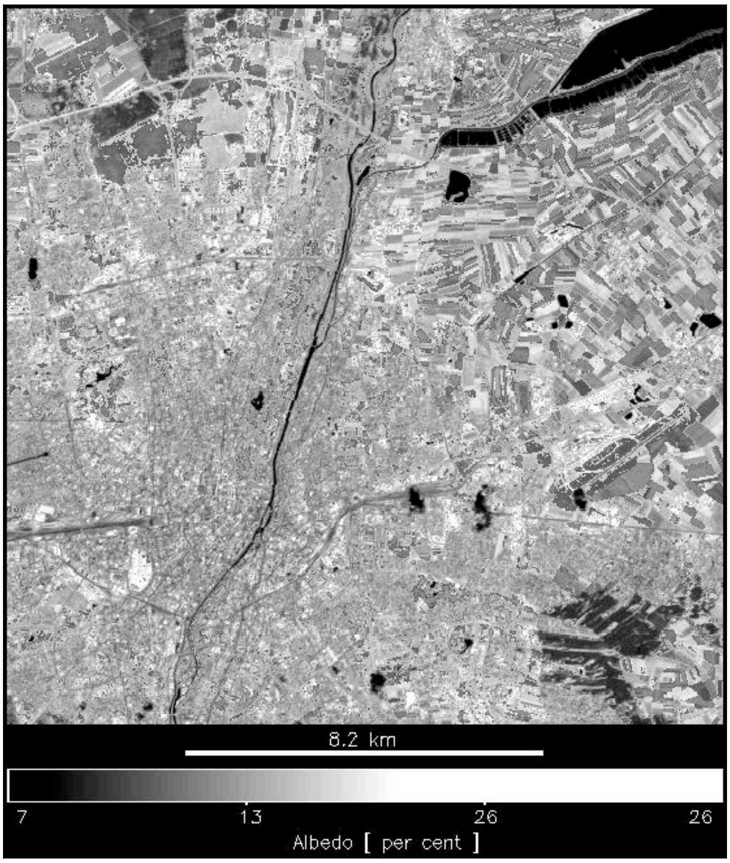

Figure 2.9 Surface albedo channel (30 m resolution of bands in the solar region).

3. Surface Energy Balance

Surface energy balance is an essential part of climatology. The energy balance equation applicable to most land surfaces can be written as (Asrar 1989)

$$R_n = G + H + LE \quad (3.1)$$

where R_n is the net radiant energy absorbed by the surface. The net energy is dissipated by conduction into the ground (G), convection to the atmosphere (H), and available as latent heat of evaporation (LE). The amount of energy employed in photosynthesis in case of vegetated surfaces is usually small compared to the other terms. Therefore, it is neglected here.
The terms on the right hand side of equation (3.1) are called heat fluxes. The soil or ground heat flux (G) ranges typically from about 10 to 50% of net radiation. Convection to the atmosphere is called sensible heat flux (H). It may warm or cool the surface depending on whether the air is warmer or cooler than the surface.
The energy available to evaporate water from the surface (LE) is usually obtained as the residual to balance the net radiation with the dissipation terms.

Net radiation is expressed as the sum of three radiation components :

$$R_n = R_{solar} + R_{atm} - R_{surface} \quad (3.2)$$

where R_{solar} is the absorbed shortwave solar radiation (0.3-3 μm), R_{atm} is the longwave radiation (3-14 μm) emitted from the atmosphere toward the surface, and $R_{surface}$ is the longwave radiation emitted from the surface into the atmosphere.

The absorbed solar radiation can be calculated as

$$R_{solar} = \int_{0.3\mu m}^{2.5\mu m} \left(1 - \rho(\lambda)\right) E_g(\lambda)\, d\lambda \quad (3.3)$$

where $\rho(\lambda)$ is the ground reflectance, $1 - \rho(\lambda)$ is the absorbed part of radiation, and $E_g(\lambda)$ is the global (direct plus diffuse) solar flux on the ground. The numerical calculation of equation (3.3) is based on the same assumptions regarding the extrapolation of bands and interpolation of gap regions as discussed in chapter 2 dealing with the ground albedo.
If the satellite imagery contains no thermal band(s) from which ground temperature can be derived, then R_{solar} is the only surface energy component that can be evaluated.

With thermal bands a ground temperature or at least a ground brightness temperature image can be derived. In this case, the emitted surface radiation can be calculated as

$$R_{surface} = \varepsilon_s \, \sigma \, T_s^4 \quad (3.4)$$

where ε_s is the surface emissivity, $\sigma = 5.669 \times 10^{-8}\ W\ m^{-2}\ K^{-4}$ is the Stefan-Boltzmann constant, and T_s is the kinetic surface temperature.
For sensors with a single thermal band such as Landsat TM an assumption has to be made about the surface emissivity to obtain the surface temperature. Usually, ε_s is selected in the range ε_s=0.95-1, and the corresponding temperature is a brightness temperature. A choice of ε_s=0.97 or ε_s=0.98 is often selected for spectral bands in the 10-12 μm region. It introduces an acceptable small temperature error of about 1-2 °C for surfaces in the

emissivity region 0.95-1. Examples are vegetated or partially vegetated fields (ε_s=0.96-0.99), agricultural soil (ε_s=0.95-0.97), water (ε_s=0.98), asphalt and concrete (ε_s=0.95-0.96). Sand and rocks can have significantly lower emissivity values (ε_s=0.80-0.90). Emissivities of various surfaces are documented in Buettner and Kern 1965, Wolfe and Zissis 1985, Sutherland 1986, Salisbury and D'Aria 1992.

The atmospheric longwave radiation R_{atm} emitted from the atmosphere toward the ground can be written as

$$R_{atm} = \varepsilon_a \, \sigma \, T_a^4 \tag{3.5}$$

where ε_a is the air emissivity, σ is the Stefan-Boltzmann constant, and T_a is the air temperature at screen height (2 m above ground, sometimes 50 m above ground are recommended). For cloud-free conditions, Brutsaert's (1975) equation can be used to predict the effective air emissivity as

$$\varepsilon_a = 1.24 \cdot \left(\frac{p_{wv}}{T_a} \right)^{1/7} \tag{3.6}$$

where p_{wv} is the water vapor partial pressure in millibars, and T_a the air temperature in Kelvin. The following figure shows p_{wv} as a function of air temperature for relative humidities of 20 – 100%. The pressure is calculated as :

$$p_{wv} = RH \; e_s \; / \, 100 \tag{3.7}$$

where RH is the relative humidity in per cent, and e_s is the water vapor pressure in saturated air (Murray 1967) :

$$e_s(T) = e_{s0} \; exp \left[\frac{a \left(T - 273.16 \right)}{T - b} \right] \tag{3.8}$$

The constants are a=17.26939, b=35.86, and $e_{s0} = e_s(T = 273.16K) = 6.1078$ mbar. T is the air temperature in Kelvin.
An alternative to eq. (3.6) is the following approximation (Idso and Jackson 1969) which does not explicitely include the water vapor and holds for average humidity conditions:

$$\varepsilon_a = 1 - 0.261 * exp \left\{ -7.77 * 10^{-4} * (273 - T_a)^2 \right\} \tag{3.6a}$$

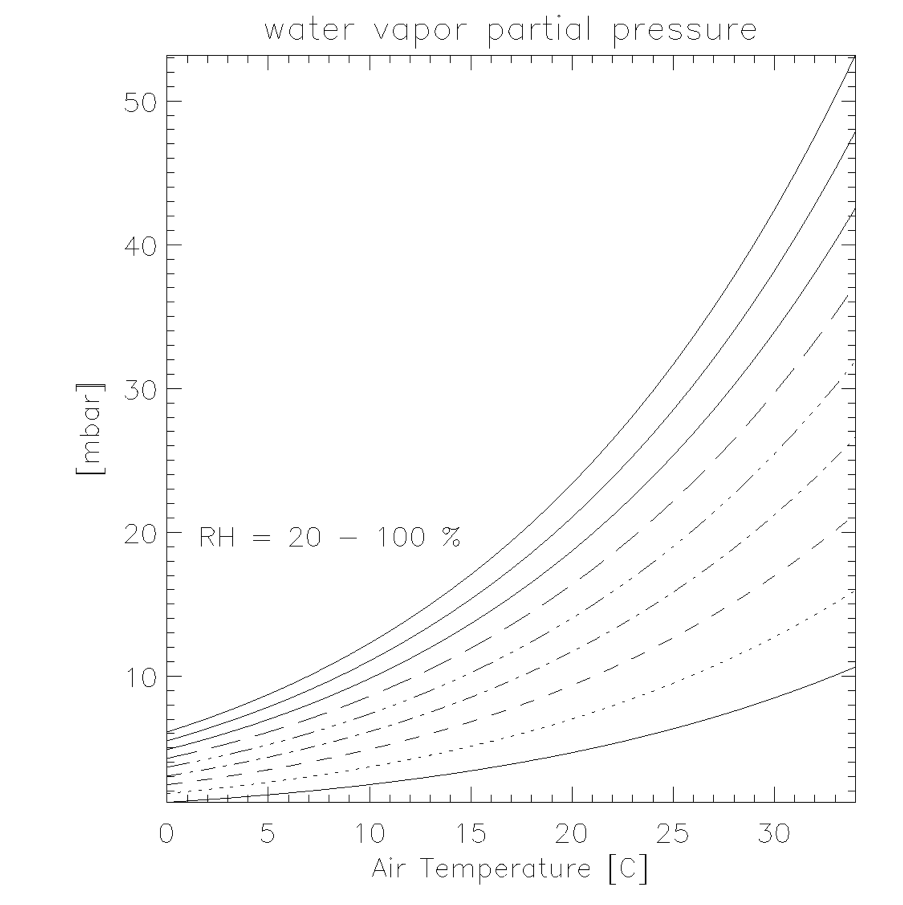

Figure 3.1. Water vapor partial pressure as a function of air temperature and humidity. Relative humidities are 20% to 100% with a 10% increment.

Table 3.1 contains selected values of ε_a as a function of T_a and p_{wv}.

T_a (°C)	p_{wv} (mbar)	RH (%)	u($g\ cm^{-2}$)	ε_a
5	5	57	0.66	0.70
	6	69	0.79	0.72
	7	80	0.92	0.73
15	5	30	0.63	0.70
	10	59	1.25	0.77
	15	88	1.87	0.81
20	10	43	1.22	0.77
	15	64	1.83	0.81
	20	86	2.44	0.85
25	20	63	2.40	0.84
	25	79	3.00	0.87
	30	95	3.60	0.89
30	25	59	2.92	0.87
	30	71	3.52	0.89
	35	82	4.10	0.91

Table 3.1 Air emissivity as a function of water vapor partial pressure and air temperature.

For comparison, relative humidity (RH) and water vapor column values u are given for a horizontal path of 1.7 km, which corresponds approximately to the 0-100 km water vapor column for standard meteorological conditions (MODTRAN atmospheres such as US standard, midlatitude summer, tropical etc.).

The ATCOR models generate a file "*flx" that contains the channels described in chapter 2 and the following radiation and heat flux channels, in total ten channels, coded with 2 bytes per pixel:

1. Soil adjusted vegetation index SAVI
2. Leaf area index LAI
3. Fraction of absorbed photosynthetically active radiation FPAR
4. Surface albedo a (integrated from 0.3 – 2.5 μm)
5. Absorbed solar radiation flux R_{solar} $(W\ m^{-2})$
6. Thermal flux difference $R_{therm} = R_{atm} - R_{surface}$ $(W\ m^{-2})$
7. Ground heat flux G $(W\ m^{-2})$
8. Sensible Heat H $(W\ m^{-2})$
9. Latent heat of evaporation LE $(W\ m^{-2})$
10. Net radiation R_n $(W\ m^{-2})$

Channels 6 – 10 are only available if surface temperature data from a thermal band exist.

Note :

If surface temperature data are not available, R_{solar} may be used as a rough approximation for R_n if estimated surface temperatures deviate less than 5°C from the air temperature. As an example, for T_a =25°C , ε_a =0.87 , and ε_s =0.98 the difference $R_{therm} = R_{atm} - R_{surface}$ is smaller than 80 $(W\ m^{-2})$ and R_{solar} ranges typically from 600 to 800 $(W\ m^{-2})$, so in these cases R_{solar} and R_n agree within about 10 - 15 per cent.

The heat fluxes G, H, and LE on the right hand side of equation (3.1) are calculated for land surfaces employing a simple parametrization with the SAVI and scaled NDVI indices (Choudhury 1994, Carlson et al. 1995) :

$$G = R_n \cdot 0.4 \cdot (SAVI_m - SAVI) / SAVI_m \tag{3.9}$$

where $SAVI_m$ = 0.814 is full vegetation cover.

$$H = B\,(T_s - T_a)^n \tag{3.10}$$

$$B = 286 \cdot (0.0109 + 0.051 \cdot NDVI^*) \tag{3.10a}$$

$$n = 1.067 - 0.372 \cdot NDVI^* \tag{3.10b}$$

$$NDVI^* = \frac{\rho_{NIR} - \rho_{RED}}{\rho_{NIR} + \rho_{RED}} / 0.75 \tag{3.10c}$$

Equation (3.10) corresponds to equation (1a) of Carlson et al. (1995), because G is neglected there, and so $R_n - G$ represents the energy left for evapotranspiration. The factor 286 in equation (3.10a) converts the unit (cm / day) into ($W\ m^{-2}$). $NDVI^*$ is the scaled NDVI. Equation (3.10c) corresponds to equation (3) of Carlson et al. (1995) with $NDVI_0 = 0$ (bare soil) and $NDVI_s = 0.75$ (full vegetation cover). The approach was developed for vegetated surfaces.

The latent heat flux LE is computed as the residual :

$$LE = R_n - G - H \tag{3.11}$$

All radiation and heat fluxes are calculated in units of ($W\ m^{-2}$). They represent instantaneous flux values. For applications where daily (24 h) LE values are required the following equation can be used for the unit conversion:

$$LE\,(\frac{cm}{day}) = \frac{1}{286}\,LE\,(W\ m^{-2}) \tag{3.12}$$

The latent heat flux LE is frequently called evapotranspiration (ET). Although LE and ET are used interchangeably the unit (cm/day) or (mm/day) is mostly employed for ET.
For water surfaces the distribution of net radiation into G, LE, and H is difficult to determine. Therefore, G and H are set to zero here, and so LE equals R_n.
Since the approach was developed for vegetated surfaces, there is a problem in applying these equations to urban areas where the vegetation index is low. In this case the sensible heat H calculated with equations (3.10) is rather low and so the latent heat LE is very high. The following figure presents a typical situation with a net radiation of 600 $W\ m^{-2}$. The top left graph shows the ground heat flux as

a function of the SAVI computed with equation (3.9), the top right shows the flux remaining for LE + H. The bottom left graph contains the latent heat flux according to equations (3.11) where the different curves correspond to five different temperatures of $T_s - T_a$ = -10, -5, 0, 5, 10°C marked with the symbols plus, asterisk, no symbol, diamond, and triangle, respectively. The plus sign represents $T_s - T_a$ = -10°C (surface temperature lower than air temperature), the triangle represents $T_s - T_a$ = +10°C (surface temperature higher than air temperature). The shaded region indicates SAVI < 0.05 (equivalent to scaled NDVI < 0.14 in this example with ρ(red)=0.10, ρ(NIR)=0.10, 0.12, 0.14, etc.). For $T_s - T_a$ = +10°C and SAVI=0 (i.e., urban area with asphalt, concrete, or buildings) the latent heat LE is 320 $W\ m^{-2}$ and H is 30 $W\ m^{-2}$, so LE is overestimated and H is underestimated. More realistic values would be LE = 30 - 60 $W\ m^{-2}$ and H = 320 - 290 $W\ m^{-2}$.

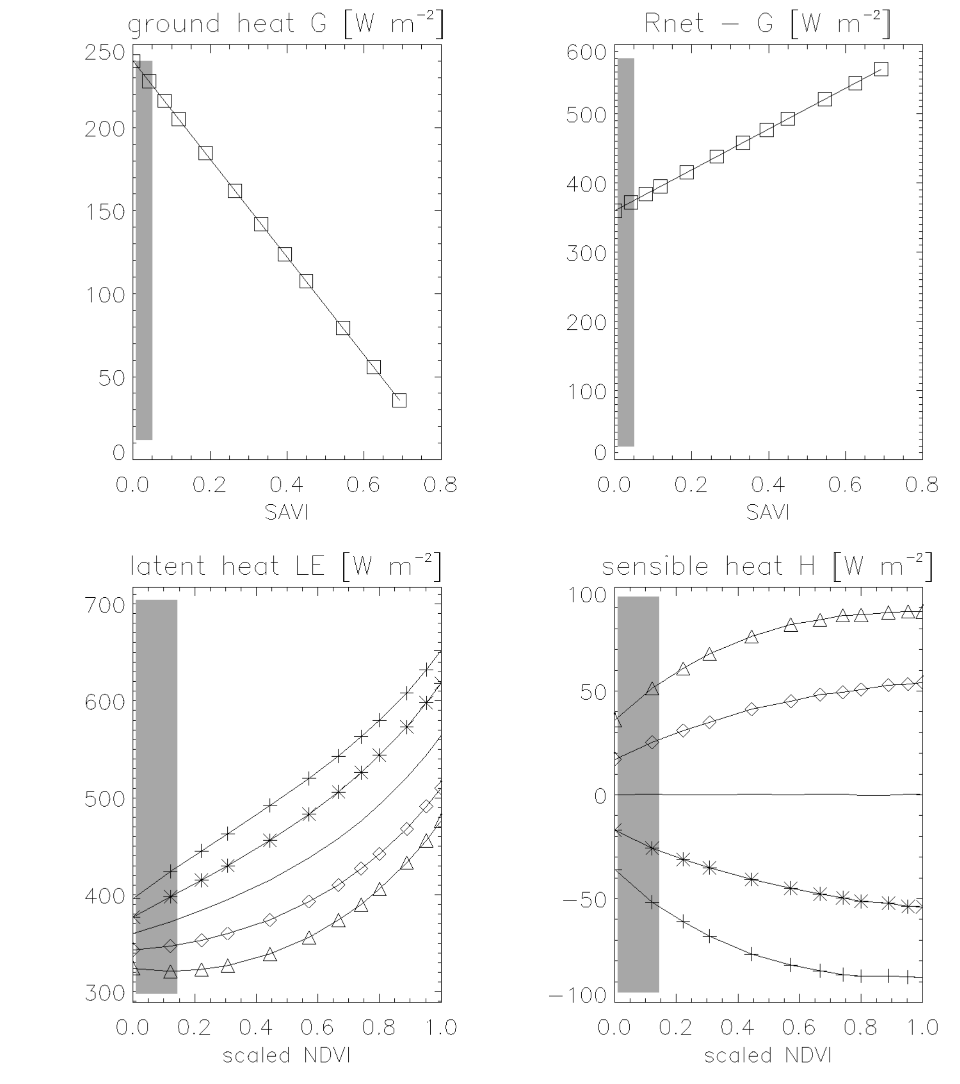

Figure 3.2 Heat fluxes as a function of vegetation index.

Spatial maps of air temperature (equation 3.10) and air emissivity (equations 3.5, 3.6) can also be included in the processing. Usually, isolated point-like measurements of air temperature are available from meteorological stations. These have to be interpolated to generate a spatial map coregistered to the image prior to applying the ATCOR model. Data in the file containing the air temperature must have the Celsius unit, data of the emissivity file must range between 0 and 1.

In case of mountainous terrain the air temperature $T_a(z_0)$ and water vapor partial pressure $p_{wv}(z_0)$ at a reference elevation z_0 have to be specified. The height dependence of air temperature is then obtained with linear extrapolation employing a user-specified adiabatic temperature gradient $\partial T / \partial z$:

$$T_a(z) = T_a(z_0) + \frac{\partial T}{\partial z}\left(z_0 - z\right) \tag{3.13}$$

where $\partial T / \partial z$ is typically in the range 0.65 – 0.9 (Celsius / 100 m). The water vapor pressure is extrapolated exponentially according to :

$$p_{wv}(z) = p_{wv}(z_0) \cdot 10^{-(z - z_0)/z_s} \tag{3.14}$$

where z_s is the water vapor scale height (default: z_s = 6.3 km).

3.1 Landsat-5 TM scene (ALPMON 1985)

Figures 3.3 to 3.6 show example imagery of R_{solar} , G, LE, and H for the Landsat TM scene of the title imagery. These figures correspond to figures 2.1 to 2.4. The net radiation channel is shown on the title page.

Figure 3.3 Absorbed solar radiation.

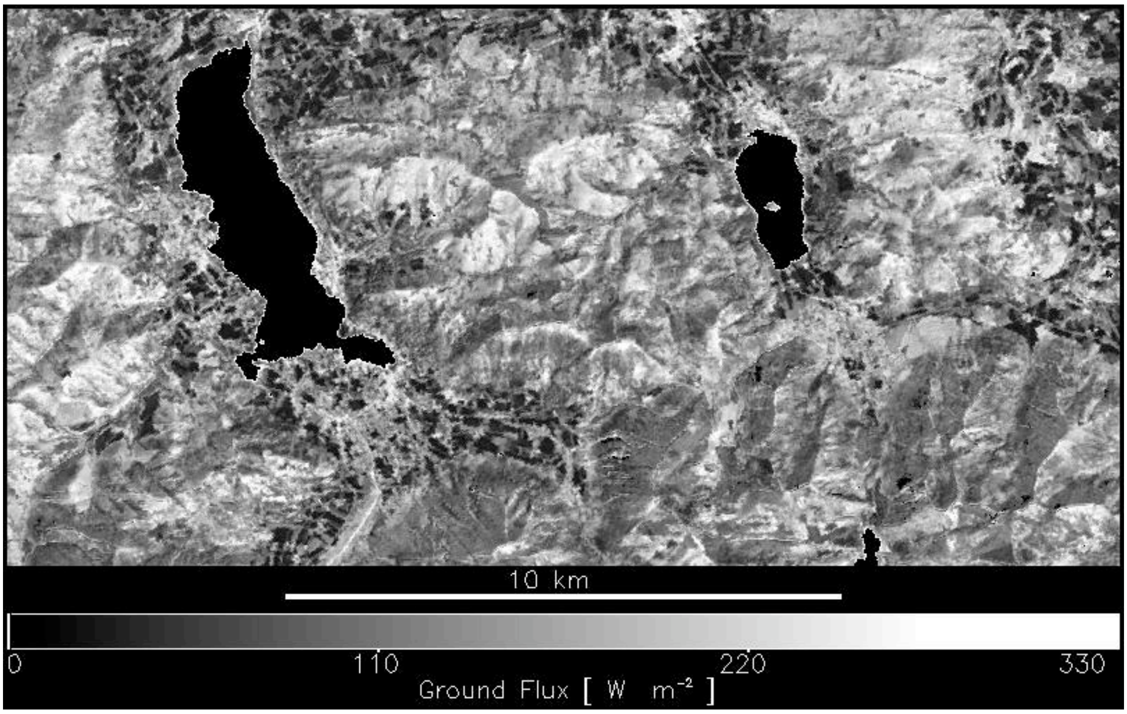

Figure 3.4 Ground heat flux.

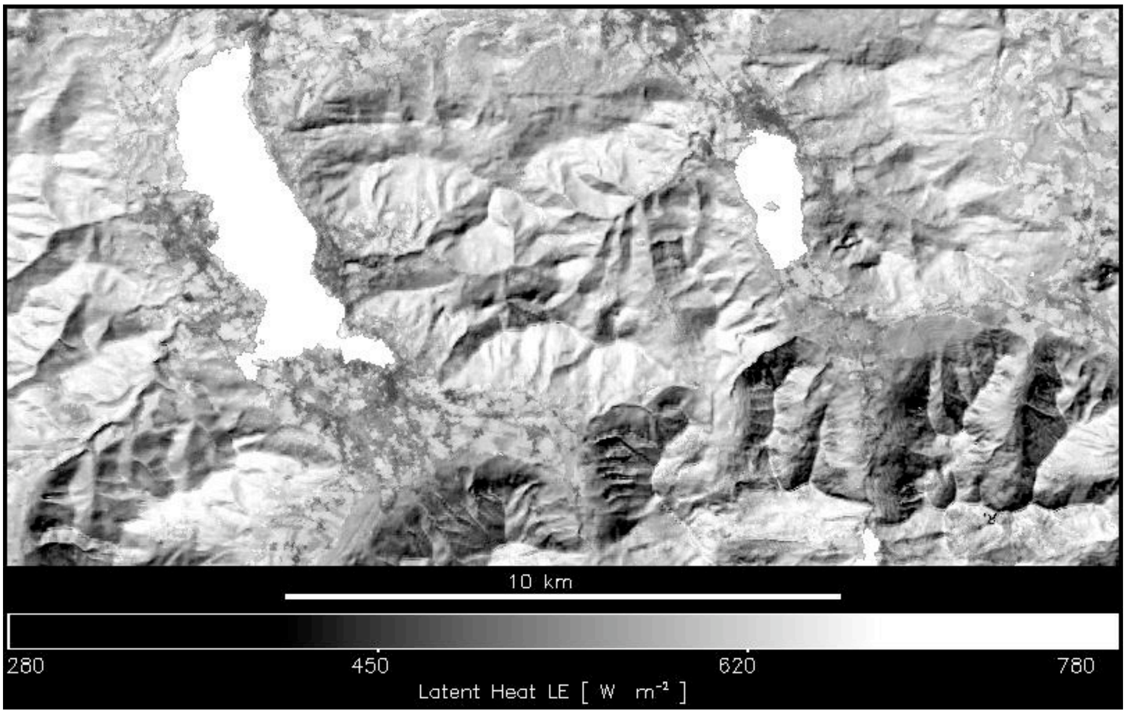

Figure 3.5 Latent heat of evaporation.

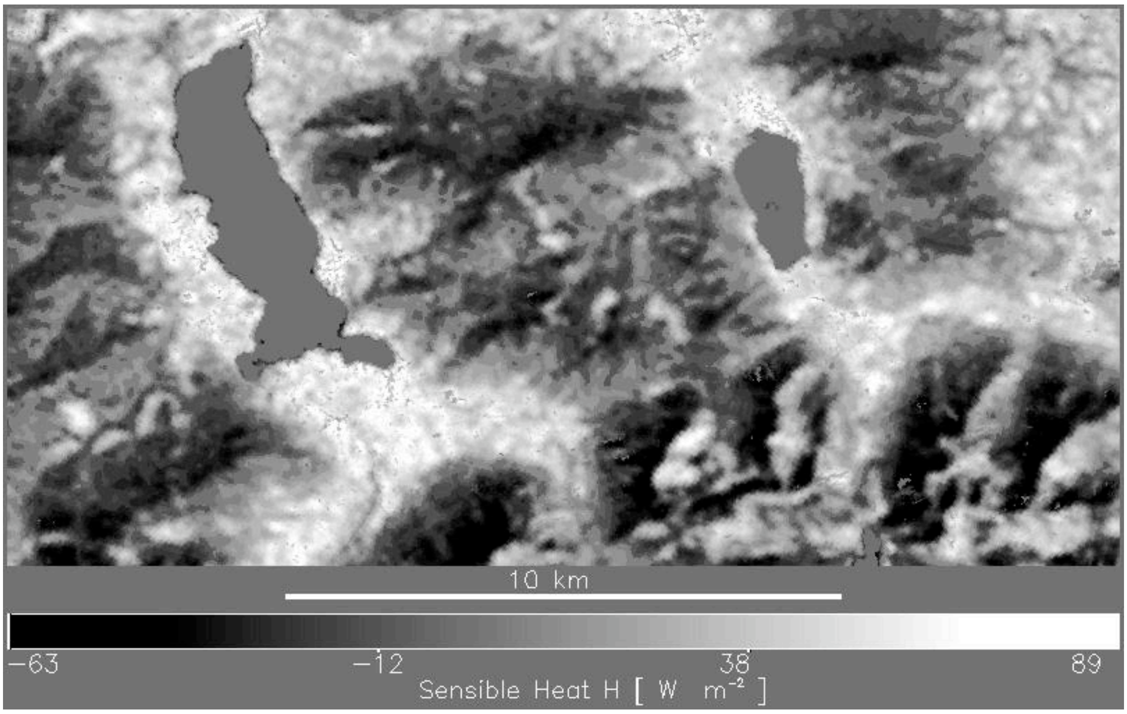

Figure 3.6 Sensible heat flux.

The scene-average air temperature was taken as 25°C. Note that for water surfaces G=H=0 is assumed, so the latent heat equals the net radiation (LE= R_n) as mentioned in chapter 3. The coarse resolution of the sensible heat flux image is caused by the 120 m spatial resolution of the thermal band of TM.

3.2 Landsat-5 TM scene (Munich 1991)

Figures 3.7 to 3.10 show example imagery of R_n, G, LE, and H for the Landsat TM scene of Figure 2.5. The scene-average air temperature was taken as 20°C. Once again, note that for water surfaces G=H=0 is assumed, so the latent heat equals the net radiation (LE=R_n).

Figure 3.7 Net radiation.

Figure 3.8 Ground heat flux.

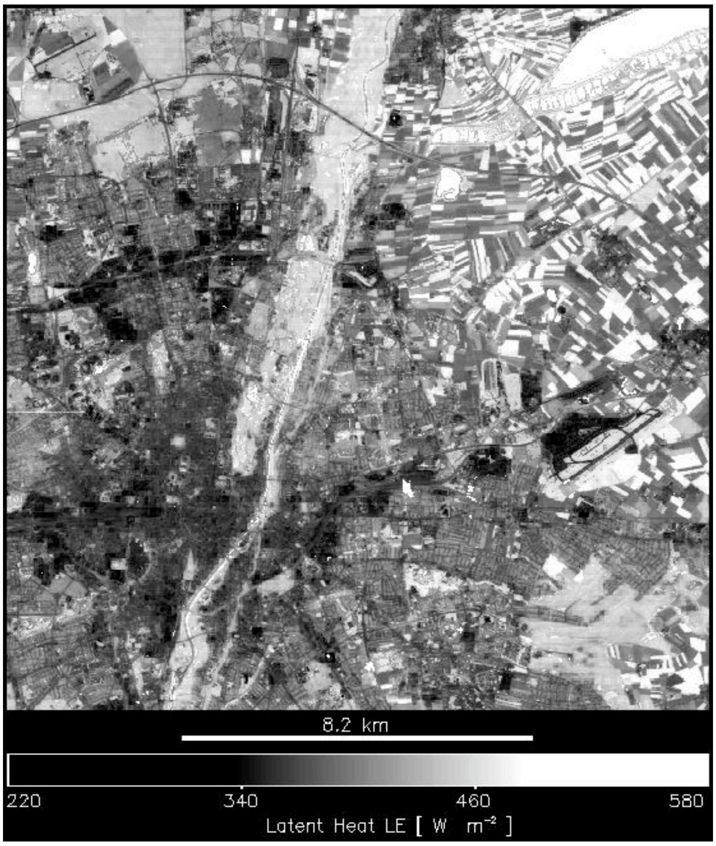

Figure 3.9 Latent heat flux.

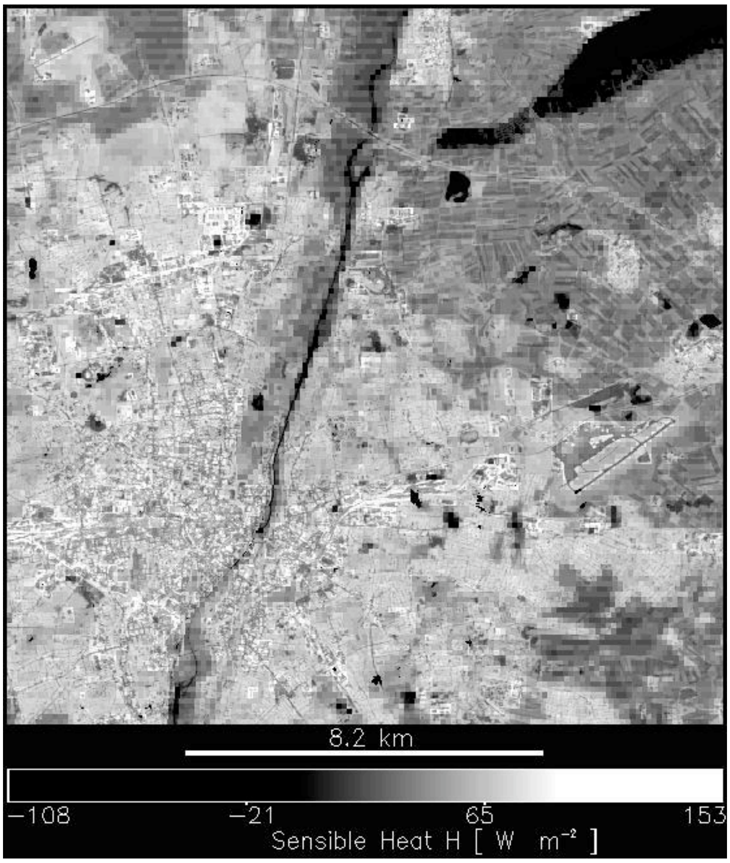

Figure 3.10 Sensible heat flux.

4. Summary

The ATCOR models have been enhanced and include an option to calculate value adding channels in a separate file. These channels are :

1. Soil adjusted vegetation index SAVI
2. Leaf area index LAI
3. Fraction of absorbed photosynthetically active radiation FPAR
4. Surface albedo a (integrated from 0.3 – 2.5 μm)
5. Absorbed solar radiation flux R_{solar} $(W\ m^{-2})$
6. Thermal flux difference $R_{therm} = R_{atm} - R_{surface}$ $(W\ m^{-2})$
7. Ground heat flux G $(W\ m^{-2})$
8. Sensible heat $(W\ m^{-2})$
9. Latent heat LE $(W\ m^{-2})$
10. Net radiation R_n $(W\ m^{-2})$

Results were presented for two selected Landsat TM scenes. The results are reasonable and show the expected trends. A quantitative comparison with simultaneous field measurements was not possible for the retrospective ALPMON monitoring project but is intended for future projects. The current approach for the calculation of the sensible and latent heat fluxes is restricted to vegetated surfaces.

5. References

ALPMON project, 1996, “Inventory of alpine-relevant parameters for an alpine monitoring system using remote sensing data”, EC, DG XII, CEO Contract ENV4-CT96-0359, testsite Mangfallgebirge of the Institute for Land Use Planning and Nature Conservation.

Asrar, G., Fuchs, M., Kanemasu, E. T., and Hatfield, J. L., 1984, Estimating absorbed photosynthetically active radiation and leaf area index from spectral reflectance in wheat, Agron. J., Vol. 76, 300-306.

Asrar, G., (Editor), 1989, Theory and applications of optical remote sensing, J. Wiley & Sons, New York.

Baret, F., and Guyot, G., 1991, Potentials and limits of vegetation indices for LAI and APAR assessment, Remote Sensing of Environment, Vol. 35, 161-173.

Brutsaert, W., 1975, On a derivable formula for long-wave radiation from clear skies, Water Resources Research, Vol. 11, 742-744.

Buettner, K. J. K., and Kern, C. D., 1965, The determination of infrared emissivities of terrestrial surfaces, Journal of Geophysical Research, Vol. 70, 1329-1337.

Carlson, T. N., Capehart, W. J., and Gillies, R. R., 1995, A new look at the simplified method for remote sensing of daily evapotranspiration, Remote Sensing of Environment, Vol. 54, 161-167.

Choudhury, B. J., 1994, Synergism of multispectral satellite observations for estimating regional land surface evaporation, Remote Sensing of Environment, Vol. 49, 264-274.

Choudhury, B. J., Ahmed, N. U., Idso, S. B., Reginato, R. J., and Daughtry, C. S. T.,1994, Relations between evaporation coefficients and vegetation indices studied by model simulations, Remote Sensing of Environment, Vol. 50, 1-17.

Huete, A. R., 1988, A soil adjusted vegetation index (SAVI), Remote Sensing of Environment, Vol. 25, 295-309.

Idso, S. B., and Jackson, R. D., 1969, Thermal radiation from the atmosphere, J. Geophysical Research, Vol. 74, 5397-5403.

Murray, F. W., 1967, On the computation of saturation vapor pressure, J. Applied Meteorology, Vol. 6, 203-204.

Richter, R., 1996, A spatially adaptive fast atmospheric correction algorithm, International Journal of Remote Sensing, Vol. 17, 1201-1214.

Richter, R., 1997, Correction of atmospheric and topographic effects for high spatial resolution satellite imagery, International Journal of Remote Sensing, Vol. 18, 1099-1111.

Richter, R., 1998, Correction of satellite imagery over mountainous terrain, Applied Optics, Vol. 37, 4004-4015.

Richter, R. 2003a, Atmospheric / topographic correction for satellite imagery, DLR-IB 564-01/03, DLR Wessling, Germany.

Richter, R. 2003b, Atmospheric/ topographic correction for airborne imagery, DLR-IB 564-02/03, DLR Wessling, Germany.

Salisbury, J. W., and D’Aria, D. M., 1992, Emissivity of terrestrial materials in the 8-14 μm atmospheric window, Remote Sensing of Environment, Vol. 42, 83-106.

Sutherland, R. A., 1986, Broadband and spectral emissivities (2-18 μm) of some natural soils and vegetation, Journal of Atmospheric and Oceanic Technology, Vol. 3, 199-202.

Wiegand, C. L., Gerbermann, A. H., Gallo, K. P., Blad, B. L., and Dusek, D., 1990, Multisite analyses of spectral-biophysical data for corn, Remote Sensing of Environment, Vol. 33, 1-16.

Wiegand, C. L., Richardson, A. J., Escobar, D. E., and Gerbermann, A. H., 1991, Vegetation indices in crop assessments, Remote Sensing of Environment, Vol. 35, 105-119.

Wolfe, W. L., and Zissis, G. J., 1985, The Infrared Handbook, Office of Naval Research, Washington, DC.